Science Advances
AAAS

# Supplementary Materials for

## Multiscale dynamical symmetries and selection rules in nonlinear optics

Gavriel Lerner *et al.*

Corresponding author: Gavriel Lerner, gavrielerner@gmail.com; Oren Cohen, oren@technion.ac.il

*Sci. Adv.* **9**, eade0953 (2023)
DOI: 10.1126/sciadv.ade0953

**This PDF file includes:**

**1) DSs of the induced polarization arising from DSs of the driver field**

We will show here how, and in under which physical conditions, the multi-scale DSs of the driver field are transferred to the induced polarization. The dynamics of an electronic (with N electrons) wave function of a system with the Hamiltonian in eq. (4) of the main text, $\psi_{\vec{R}}(\vec{r}_1, \vec{r}_2, \dots, \vec{r}_N, t)$, is governed by the following TDSE:

$$i\frac{\partial}{\partial t}\psi_{\vec{R}}(\vec{r}_1, \dots, \vec{r}_N, t) = \left[\sum_j \frac{\nabla_j^2}{2} + \frac{1}{2}\sum_{i\neq j}\left|\vec{r}_i - \vec{r}_j\right|^{-1} + \sum\nolimits_j U_{\vec{R}}(\vec{r}_j) + \sum_j \vec{E}(\vec{R}, t)\cdot\vec{r}_j\right]\psi_{\vec{R}}(\vec{r}_1, \dots, \vec{r}_N, t) \quad (1)$$

Applying the coordinate transformation, $\vec{r}_j \to \hat{\gamma}\vec{r}_j$ (i.e., a point group operation, $\hat{\gamma}$, operating on the microscopic space), and time transformation, $t \to st + \tau$, where $\tau$ is the time translation and $s = \pm 1$ (-1 for time-reversal), on eq. (1) yields

$$i\frac{\partial}{\partial t}\psi_{\vec{R}}(\hat{\gamma}\vec{r}_1, \dots, \hat{\gamma}\vec{r}_N, st + \tau) = \left[\sum_j \frac{\nabla_j^2}{2} + \frac{1}{2}\sum_{i\neq j}\left|\hat{\gamma}\vec{r}_i - \hat{\gamma}\vec{r}_j\right|^{-1} + \sum\nolimits_j U_{\vec{R}}(\hat{\gamma}\vec{r}_j) + \sum_j \vec{E}(\vec{R}, st + \tau)\cdot\hat{\gamma}\vec{r}_j\right]\psi_{\vec{R}}(\hat{\gamma}\vec{r}_1, \dots, \hat{\gamma}\vec{r}_N, st + \tau) \quad (2)$$

If the electric field is conserved under the multi-scale DS (i.e., $\hat{\gamma}\vec{E}(\vec{R}, st + \tau) = \vec{E}(\hat{\mathrm{M}}_R\vec{R}, t)$ and the microscopic potential of the medium shares the same symmetry (i.e., the relation between the

microscopic static potential in points $\vec{R}$ and $\widehat{\mathrm{M}}_R\vec{R}$ is $U_{\vec{R}}(\hat{\gamma}\vec{r}) = U_{\widehat{\mathrm{M}}_R\vec{R}}(\vec{r})$, as is the case with homogeneous and isotropic media), then:

$$i\frac{\partial}{\partial t}\psi_{\vec{R}}(\hat{\gamma}\vec{r}_1,\dots,\hat{\gamma}\vec{r}_N,st+\tau) = \left[\sum_j \frac{\nabla_j^2}{2} + \frac{1}{2}\sum_{i\neq j}\left|\vec{r}_i-\vec{r}_j\right|^{-1} + \sum\nolimits_j U_{\widehat{\mathrm{M}}_R\vec{R}}(\vec{r}_j) + \sum_j \vec{E}\left(\widehat{\mathrm{M}}_R\vec{R},t\right)\cdot\vec{r}_j\right]\psi_{\vec{R}}(\hat{\gamma}\vec{r}_1,\dots,\hat{\gamma}\vec{r}_N,st+\tau) \quad (3)$$

such that

$$i\frac{\partial}{\partial t}\widehat{G'}\psi_{\vec{R}}(t) = \widehat{H}_{\widehat{\mathrm{M}}_R\vec{R}}(t)\widehat{G'}\psi_{\vec{R}}(t) \quad (4)$$

where $\widehat{G'}$ is a unitary (or antiunitary, in the case of time reversal) transformation of time and microspace, where $\widehat{G'}\ \widehat{\mathrm{M}}_R = \hat{G}$. Now, if we look at the full Hamiltonian of the non-interacting microscopic systems, $\widehat{H}(t) = \sum_{\vec{R}}\widehat{H}_{\vec{R}}(t)$, which describes the dynamics of the full wave function of non-interacting microscopic systems, $\psi(t) = \prod_{\vec{R}}\psi_{\vec{R}}(t)$, we see that according to eq. (4), the full Hamiltonian is conserved under the multi-scale DS:

$$\hat{G}\widehat{H}(t)\hat{G}^{-1} = \sum_{\vec{R}}\widehat{G'}\ \widehat{H}_{\widehat{\mathrm{M}}_R\vec{R}}(t)\,\hat{G}'^{\ -1} = \sum_{\vec{R}}\widehat{H}_{\vec{R}}(t) = \widehat{H}(t) \quad (5)$$

Therefore we can use Floquet theory in a similar manner as in (*13*). For a periodic Hamiltonian (if the EM field is aperiodic with multiple frequencies, then the system can by described by the many-mode Floquet state theory(*45*, *46*)), $\widehat{H}(t+T) = \widehat{H}(t)$, and the Floquet Hamiltonian, $\mathcal{H}_F = \widehat{H}(t) - i\frac{\partial}{\partial t}$, has eigenstates which are T-periodic Floquet modes, $u_n(t)$, with corresponding quasi-energies, $\varepsilon_n$. Solutions to the time-dependent Schrödinger equation (TDSE) of the full Hamiltonian, $\widehat{H}(t)$, are comprised of Floquet states $\psi_n(t) = e^{i\varepsilon_n t}u_n(t)$. If $\hat{G}\widehat{H}(t) = \widehat{H}(t)$ (eq. (5)), then $\left[\hat{G},\mathcal{H}_F\right] = 0$, such that the Floquet modes are simultaneous eigenmodes of the Floquet Hamiltonian and $\hat{G}$. Furthermore, since $\hat{G}$ is unitary or anti-unitary, its eigenvalues are roots of unity; $\hat{G}u_n(t) = e^{i\phi_n}u_n(t)$, where $\phi_n$ is real. Hence, if the initial wave function populates a single Floquet state, any measured observable (e.g. the induced polarization), $o\left(\vec{R},t\right) = \left\langle u(t)\middle|\hat{O}\middle|u(t)\right\rangle = \left\langle u(t)\middle|\sum_{\vec{R}}\hat{O}_{\vec{R}}\middle|u(t)\right\rangle$, also upholds the DS:

$$o\left(\vec{R},t\right) = \left\langle u(t)\middle|\hat{G}^{-1}\hat{G}\hat{O}\hat{G}^{-1}\hat{G}\middle|u(t)\right\rangle = \hat{G}o\left(\vec{R},t\right) \quad (6)$$

The EM field is often a pulse with finite duration, so the requirement becomes that the wave function before the pulse exhibits the DS, which is the case for an isotropic gas in the ground state. The pulse should be turned on adiabatically to approximately initiate steady-state dynamics of a single Floquet state (*47*). Another requirement is that the temporal frequencies of the driver and HHG emission are not close to a resonance frequency of the potential, $U$ (*47*). Also, if the initial state is not a single Floquet mode, but a superposition of Floquet modes, eq. (6) will not hold unless the medium consists of an isotropic ensemble that contains an equal population of all degenerate states (*13*). Under the above conditions, the symmetry of the field, $\vec{E}\left(\widehat{\mathrm{M}}_R\vec{R},t\right) = \widehat{G'}\ \vec{E}\left(\vec{R},t\right)$, is transferred to the induced polarization, $\vec{P}\left(\widehat{\mathrm{M}}_R\vec{R},t\right) = \widehat{G'}\ \vec{P}\left(\vec{R},t\right)$.

Notably, the above discussion did not include macroscopic effects that could also affect the symmetry-relations and possible break the symmetry (e.g. due to phase-matching, spatial averaging, etc.). They are discussed in the next section.

**2) Selection rules in the induced polarization and their appearance in the far field of the HHG**

In the main text, we discussed how DSs lead to selection rules in the Fourier components of the induced polarization. Here we discuss and analyze how this selection will appear in the far field of the harmonic generation, which is measured in HHG experiments.

We first discuss the macroscopic conditions under which the DSs of the driver field are transferred to the induced polarization. The principle condition is that the entire system (driver field and medium) should be conserved under the multi-scale DSs. Imperfections in these symmetries (e.g., due to non-uniform density of the gas) lead to deviations from the symmetry and selection rules. In a case where the symmetry includes propagation, in order that the driver field will be periodic in the propagation axis, it needs to be approximately non-depleted and loosely focused (such that the Rayleigh length of the focusing beam is larger than the interaction length). We point out that the driver field (i.e., $\vec{E}(\vec{R},t)$) is the field inside the interaction region which is sensitive to the medium dispersion. Moreover, phase mismatch between the induced polarization and emitted harmonic field can alter the transfer of the selection rules to the far field.

Now we will analyze how the selection rules in the Fourier components of the induced polarization will appear in the far field of the harmonic generation. The induced polarization radiates the HHG field, $\vec{E}_{HHG}$, according to the inhomogeneous wave equation:

$$\left(\nabla^2-\frac{1}{c^2}\partial_t^2\right)\vec{E}_{HHG}(X,Y,Z,t)=\frac{4\pi}{c^2}\partial_t^2\vec{P}(X,Y,Z,t) \tag{7}$$

This equation can be solved numerically using the discrete dipole approximation (*48*). The detection of the harmonics is typically performed at approximately one-meter scale after the interaction region, and the diameter of the detector is several centimeters. (In many HHG setups there is also a small aperture between the interaction region and the detector which also restricts the detection to small divergence.) Therefore, the detection captures the far-field of the HHG emission which can be approximated by the Fraunhofer diffraction equation for each Z slice of the interaction region with a total length, $L$:

$$\vec{E}_{HHG}(x_d,y_d,\omega)\simeq\int_0^L dZ\frac{k^2e^{ik(z_d-Z)}e^{\frac{ik\left(x_d^2+y_d^2\right)}{2(z_d-Z)}}}{2\pi i(z_d-Z)}\iint dXdY e^{\frac{-ik}{z_d-Z}(x_dX+y_dY)}\vec{P}(X,Y,Z,\omega) \tag{8}$$

where $x_d$ and $y_d$ are the coordinates of the detector that is located $z_d$ distance from the interaction region, and $k$ is the wavenumber of temporal frequency, $\omega$. (Outside the interaction region $k=\omega/c$, and inside the interaction region $k=n_\omega\omega/c$ ($|n_\omega-1|\ll 1$, is typically the case in the XUV.) By using the condition $\frac{Lkx_dX}{z_d^2}\lesssim 0.01q_\omega\ll 1$, we can approximate:

$$\vec{E}_{HHG}(x_d, y_d, \omega) \approx \frac{\omega^2 e^{i\frac{\omega}{c}z_d\left(1+\frac{x_d^2+y_d^2}{2z_d^2}\right)}}{2\pi i z_d c^2}\int_0^L dZ e^{-i\frac{n_\omega \omega}{c}Z\left(1-\frac{x_d^2+y_d^2}{2z_d^2}\right)}\iint dXdY e^{\frac{-in_\omega\omega}{cz_d}(x_dX+y_dY)}\vec{P}(X,Y,Z,\omega) \quad (9)$$

The last term is the 2D far field Fourier transform with frequencies $kx_d/2\pi z_d$ and $ky_d/2\pi z_d$. This equation is easy to calculate numerically for a given $\vec{P}(X,Y,Z,\omega)$. However, the simulation of $\vec{P}(X,Y,Z,\omega)$ is difficult since it involves solving the TDSE for many $(X,Y,Z)$ points. However, by using the DS, it is enough to calculate $\vec{P}(X,Y,Z,\omega)$ only inside the spatial unit cell of the DS and then extrapolate $\vec{P}(X,Y,Z,\omega)$ outside the unit cell according to the DS. Here, we express the far field emission using the Fourier series of $\vec{P}(X,Y,Z,t)$ with a (3+1)D Gaussian envelope:

$$\vec{P}(X,Y,Z,t) = e^{-\frac{X^2}{2\sigma_X^2}-\frac{Y^2}{2\sigma_Y^2}-\frac{t^2}{2\sigma_t^2}}\sum_{\vec{k}=(k_x,k_y,k_z,\omega_q)}\vec{F}(\vec{k})\exp\big(i(k_xX+k_yY+k_zZ-\omega_q t)\big) \quad (10)$$

which plugged into eq. (9), gives:

$$\vec{E}_{HHG}(x_d, y_d, \omega) \approx \sum_{\vec{k}}\left\{\vec{F}(\vec{k})\frac{\omega^3\sigma_X\sigma_Y\sigma_t L e^{i\frac{\omega}{c}z_d\left(1+\frac{x_d^2+y_d^2}{2z_d^2}\right)}}{2\pi i z_d c^2}g_\omega(\omega - \omega_q)sinc\left(L\left(k_z-\frac{n_\omega\omega}{c}\left(1-\frac{x_d^2+y_d^2}{2z_d^2}\right)\right)\right)g_{k_x}\left(k_x-\frac{x_d}{z_d}\frac{n_\omega\omega}{c}\right)g_{k_y}\left(k_y-\frac{y_d}{z_d}\frac{n_\omega\omega}{c}\right)\right\} \quad (11)$$

where $g_\omega(\omega) = e^{-\frac{\sigma_t^2\omega^2}{2}}$, $g_{k_x}(k_x) = e^{-\frac{\sigma_X^2k_x^2}{2}}$, and $g_{k_y}(k_y) = e^{-\frac{\sigma_Y^2k_y^2}{2}}$ and $\sigma_X$, $\sigma_Y$, and $\sigma_t$ are the spatial and temporal Gaussian widths, respectively. This expression is maximal for $k_z = \frac{n_\omega\omega}{c}\left(1-\frac{x_d^2+y_d^2}{2z_d^2}\right)$, $k_x = \frac{n_\omega\omega}{c}\frac{x_d}{z_d}$, $k_y = \frac{n_\omega\omega}{c}\frac{y_d}{z_d}$, and $\omega = \omega_q$ which gives the condition of phase matching, $k_z^2+k_x^2+k_y^2 = \left(\frac{n_{\omega_q}\omega_q}{c}\right)^2$.

By considering this phase matching condition, in the case of our experiment with the tri-circular beam (as described in Fig. 3 of the main text), we can see that $k_z = \frac{q_1\omega}{c} - q_2\beta$ of the induced polarization is phased matched for $q_2\beta = \frac{q_1\omega}{c}\frac{x_d^2+y_d^2}{2z_d^2}$. Therefore, the on-axis harmonics are phase matched only for $q_2 = 0$. (Hence, the selection rule for the temporal harmonics is $q_1 = 3n \pm 1$, as was demonstrated in the experiment.) Rings with radius $\sqrt{\frac{2z_d^2q_2\beta c}{q_1\omega}}$ are also allowed (with temporal harmonic, $q_1 = 3n \pm 1 - q_2$, as was mentioned in the main text).

Another consideration is reabsorption of the emitted high harmonic field. The index of refraction in the XUV is the complex valued $n_{\omega_q} = 1 + \Delta n_{\omega_q} + i\beta_{\omega_q}$, with typical values (far from resonance) $|\Delta n_{\omega_q}| \lesssim 10^{-5}$ (*49*) and $\beta_{\omega_q} \lesssim 10^{-6}$(or $k' = \beta_{\omega_q}\frac{\omega}{c} \lesssim 1mm^{-1}$) (*50*) for 1 bar pressure. Inserting the complex valued $n_{\omega_q}$ into the $Z$-dependent part in eq. (9) gives:

$$\int_0^L dZ e^{(i\Delta k - \tilde{k})Z} = \frac{\tilde{k} + e^{-\tilde{k}L}\left(\Delta k \sin(\Delta kL) - \tilde{k}\cos(\Delta kL)\right)}{\tilde{k}^2 + \Delta k^2} \tag{12}$$

where $\Delta k = k_z - \frac{(1+\Delta n_{\omega_q})\omega}{c}\left(1 - \frac{x_d^2+y_d^2}{2z_d^2}\right)$ and $\tilde{k} = \frac{\beta_{\omega_q}\omega}{c}\left(1 - \frac{x_d^2+y_d^2}{2z_d^2}\right)$. Fig. S1 shows the amplitude of an emitted harmonic as a function of $\tilde{k}L$ and $\Delta kL$ according to eq. (12). When the absorption is small, i.e., $\tilde{k} < \Delta k, 1/L$, eq. (12) reduces to $Lsinc(\Delta kL)$. When the absorption is large, i.e., $\tilde{k} > 1/L$, eq. (12) reduces to $\frac{\tilde{k}}{\tilde{k}^2+\Delta k^2}$. This means that as $\tilde{k}L$ gets larger, the phase matching condition for $\Delta kL$ is less strict. Therefore, when the absorption is large, harmonics with larger values of $\Delta k$ can have significant amplitudes compared to harmonics with small values of $\Delta k$. In the case of our experimental example, this also means that harmonics with $q_2 = 1$ can arrive to the detector with temporal harmonics $q_1 = 3n \pm 1 - q_2$. In this case, the amplitude of the $q_1 = 3n$ harmonics will not drop completely to zero, as can be seen in fig. 3f in the main text.

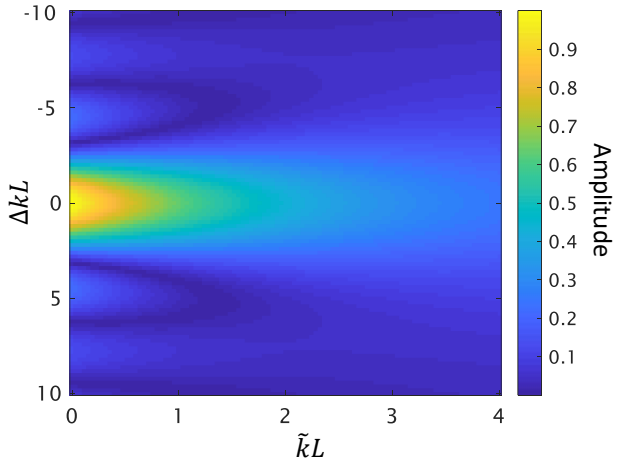


**Fig. S1. The joint effect of phase mismatch $\Delta k$ and absorption $\tilde{k}$ on the amplitude, according to eq. (12).**

3) **Constraints on the Fourier spectrum of the induced polarization from DSs in real space**

We will now prove that a general DS $\hat{G} = \hat{\gamma}\hat{M}$ leads to eq. (6) in the main text which gives constraints on the harmonics of the induced polarization $\vec{P}$ in the Fourier space.

$$\vec{P}(\vec{X}) = \hat{G}^{-1}\vec{P}(\vec{X}) = \hat{\gamma}^{-1}\vec{P}(\hat{M}\vec{X}) = \hat{\gamma}^{-1}\vec{P}(\hat{\Gamma}^{-1}\vec{X} - \vec{a}) \tag{13}$$

In the Fourier domain, this constraint reads:

$$\sum_{\vec{k}} \vec{F}(\vec{k}) \exp\left(i\vec{k}\cdot\vec{X}\right) = \sum_{\vec{k}} \hat{\gamma}^{-1}\vec{F}(\vec{k}) \exp\left(i\vec{k}\cdot(\hat{\Gamma}^{-1}\vec{X}-\vec{a})\right) \quad (14)$$

The left hand side of eq. (14) can also be written, by a change of the order of summation, as

$$\begin{aligned}\sum_{\vec{k}} \vec{F}(\hat{\Gamma}\vec{k}) \exp\left(i\hat{\Gamma}\vec{k}\cdot\vec{X}\right) &= \sum_{\vec{k}} \vec{F}(\hat{\Gamma}\vec{k}) \exp\left(i\hat{\Gamma}^{-1}\hat{\Gamma}\vec{k}\cdot\hat{\Gamma}^{-1}\vec{X}\right) \\ &= \sum_{\vec{k}} \vec{F}\left(\hat{\Gamma}\vec{k}\right) \exp\left(i\vec{k}\cdot\hat{\Gamma}^{-1}\vec{X}\right) = \sum_{\vec{k}} \hat{\gamma}^{-1}\vec{F}(\vec{k}) \exp\left(i\vec{k}\cdot(\hat{\Gamma}^{-1}\vec{X}-\vec{a})\right)\end{aligned} \quad (15)$$

Consequently, the Fourier coefficients of identical exponents $\exp\left(i\vec{k}\cdot\hat{\Gamma}^{-1}\vec{X}\right)$ in Eq. (15) must be equal and therefore $\vec{F}\left(\hat{\Gamma}\vec{k}\right) = \hat{\gamma}^{-1}\vec{F}(\vec{k})\exp\left(-i\vec{k}\cdot\vec{a}\right)$, and after multiplication with $\hat{\gamma}\exp\left(i\vec{k}\cdot\vec{a}\right)$:

$$\hat{\gamma}\vec{F}\left(\hat{\Gamma}\vec{k}\right)\exp\left(i\vec{k}\cdot\vec{a}\right) = \vec{F}(\vec{k}) \quad (16)$$

Which is Eq. (7) in the main text.

4) **Selection rules of macrospace inversion and reflection and/or time reversal**

We now derive the selection rules for symmetries that include time reversal or space reflection (rows 9-14 in table 1 in the main text for the case of (1+1+2)D).

**DS with macrospace-inversion and time reversal**

Since macrospace-inversion and time reversal (i.e. $\hat{\Gamma}\vec{X} = -\vec{X}$) is an order two operator, then the microscopic operation $\hat{\gamma}$ must be of order one or two, which can be reflection, inversion or 180 degrees rotations. Therefore, the eigenvector polarizations of $\hat{\gamma}$, $\hat{F}_i(\vec{k})$, are orthogonal linear polarizations: $\hat{F}_x(\vec{k}), \hat{F}_y(\vec{k})$, and $\hat{F}_z(\vec{k})$ (where with no loss of generality the x,y,z coordinates are chosen such that one of them is along the rotation axis or normal to the reflection plane of $\hat{\gamma}$) with possible $\alpha_i$ eigenvalues of 0 or $\pm\pi$. Since $\vec{P}(\vec{X})$ is real, $\vec{F}(-\vec{k})$ equals the complex conjugate $\vec{F}^*(\vec{k})$; therefore, $\phi_i(-\vec{k}) = -\phi_i(\vec{k})$. The phase difference between two polarizations with the same $\vec{k}$ will be:

$$\Delta\phi_{i,i'} = \phi_i(\vec{k}) - \phi_{i'}(\vec{k}) = \vec{k}\cdot\vec{a} + \alpha_i - \phi_i(\vec{k}) - \left(\vec{k}\cdot\vec{a} + \alpha_{i'} - \phi_{i'}(\vec{k})\right) = \alpha_i - \alpha_{i'} - \Delta\phi_{i,i'} \quad (17)$$

hence:

$$\Delta\phi_{i,i'} = (\alpha_i - \alpha_{i'})/2 \quad (18)$$

According to eq. (18), the phase difference between the two linear polarization components (i.e., $\Delta\phi_{i,i'}$) of the $\vec{k}$ harmonics equals $(\alpha_i - \alpha_{i'})/2$, which is expressed as either (i) a multiple of $\pi$, which means that the two linear polarization components, $\hat{F}_i(\vec{k})$ and $\hat{F}_{i'}(\vec{k})$, are in phase, and thus polarization is linear in the $i - i'$ plane; or (ii) $\pm\pi/2$, in which case all the harmonics are elliptically polarized with minor/major ellipse axes along $i$ and $i'$. Therefore, for N=2, if $\hat{\gamma}$ is the identity or $\hat{r}_2$ operation, then all the harmonics are linearly polarized (row 9 table 1 in the main text). Otherwise, if $\hat{\gamma}$ is a reflection operator, then all of the harmonics are elliptically polarized with major/minor axes corresponding to the reflection axes (row 10 in table 1 in the main text). For N=3, if $\hat{\gamma}$ is the identity or inversion operation, all harmonics are linearly polarized. Instead, if $\hat{\gamma} = \hat{r}_2$, the rotation axis is a major/minor axis of the polarization ellipsoid. If $\hat{\gamma}$ is a reflection operator, the polarization ellipsoid has a major/minor axis normal to the reflection plane.

**DS with macrospace reflection**

Now we will consider DSs that do not involve macrospace-inversion and time reversal, but require only some reflection in macrospace or time. If the DS involves a macrospace reflection, then eq. (8) in the main text becomes:

$$A_{q_1,-q_2}\exp\left(i\phi_{q_1,-q_2}+i\vec{k}\cdot\vec{a}\right)\hat{\gamma}\hat{F}_{q_1,-q_2}=A_{q_1,q_2}\exp\left(i\phi_{q_1,q_2}\right)\hat{F}_{q_1,q_2} \quad (19)$$

Therefore, the amplitudes of the mirrored spatial harmonics, $q_2$ and $-q_2$, are the same, i.e., $A_{q_1,q_2}=A_{q_1,-q_2}$. According to eq. (19), when the microscopic operation ($\hat{\gamma}$) is the identity or the inversion operations ($\pi$ rotation in 2D), $\hat{F}_{q_1,-q_2}$ must equal $\hat{F}_{q_1,q_2}$ (row 11 in table 1 in the main text). Also, if $\hat{\gamma}$ is a reflection operation, $\hat{\sigma}$, then $\hat{\sigma}\hat{F}_{q_1,-q_2}=\hat{F}_{q_1,q_2}$ (row 12 in table 1 in the main text). Eq. (19) also determines the relationship between the phases $\phi_{q_1,-q_2}$ and $\phi_{q_1,q_2}$. This relationship depends on $\hat{\gamma}$ and the propagation term, $\vec{k}\cdot\vec{a}$.

**DS with time reversal**

When the DS involves a time reversal, eq. (8) in the main text becomes:

$$A_{-q_1,q_2}\exp\left(i\phi_{q_1,-q_2}+i\vec{k}\cdot\vec{a}\right)\hat{\gamma}\hat{F}_{q_1,-q_2}=A_{q_1,q_2}\exp\left(i\phi_{q_1,q_2}\right)\hat{F}_{q_1,q_2} \quad (20)$$

Therefore, $A_{q_1,q_2}=A_{-q_1,q_2}$. When $\hat{\gamma}$ is the identity or the inversion operation ($\pi$ rotation in 2D), $\hat{F}_{-q_1,q_2}=\hat{F}_{q_1,q_2}$. Hence, the polarization must be linear (row 13 in table 1 in the main text). When $\hat{\gamma}$ is the reflection operation, $\hat{\sigma}$, then $\hat{\sigma}\hat{F}_{-q_1,q_2}=\hat{F}_{q_1,q_2}$, and the polarization ellipse axis must be orthogonal to the $\hat{\sigma}$ plane (row 14 in table 1 in the main text).

5) **Tables of macroscopic, time and microscopic building blocks operations**

In the main text we described multi-scale DS and discussed various examples. All symmetries for the (2+1+1)d case were outlined in table 1 of the main text. The number of all possible symmetries (and the number of symmetry groups) grows exponentially as the dimensionality increases. The enumeration and classification of all the symmetries and symmetry groups can be done in a similar manner as was done for magnetic groups (*51*). The building blocks operations for multi-scale DS are describe in the main text, and listed here in tow tables: table S1 for the macrospace-time operation and table S2 for microspace operations. In table S2 we also give the eigenvectors and eigenvalues which are used in the selection rules derivations.

**Table S1. Macrospace and time operation building blocks, their actions on $\vec{E}(\vec{R},t)$, and their associated order.**

| Macroscopic-time operation $\widehat{M}$ | $\widehat{M}\vec{E}(\vec{R},t)$ | Order of $\widehat{M}$ |
|---|---|---|
| Time translation, $\hat{\tau}_{n,m}$ | $\vec{E}\left(\vec{R},t+Tm/n\right)$ | $n$ |
| Space translation, $\hat{J}_{n,m}$ | $\vec{E}\left(\vec{R}+Lm/n\,\hat{\jmath},t\right)$ | $n$ |
| Macrospace-time translation, $\widehat{D}_n$ | $\vec{E}\left(\vec{R}+\frac{\vec{u}}{n},t+\tau/n\right)$ | $n$ |
| Time-reversal, $\hat{T}$ | $\vec{E}\left(\vec{R},-t\right)$ | 2 |
| Reflection, $\hat{\Sigma}_x$ | $\vec{E}(-X,Y,Z,t)$ | 2 |
| Space rotation, $\hat{R}_{n,m}$ | $\vec{E}(X',Y',Z,t)$ | $n$ |

**Table S2. Microscopic operation building blocks, e.g., reflection and rotation.** The order, matrix representation, eigenvectors, and eigenvalues of each operation is listed. The rotation angle is defined as $\theta = 2\pi m/n$. LCM is the least common multiple.

| Microscopic Operation, $\hat{\gamma}$ | Order | Matrix Representation | Eigenvectors, $\hat{F}_{\vec{n}}^{(m)}$ | Eigenvalues, $e^{i\alpha^{(m)}}$ |
|---|---|---|---|---|
| Reflection, $\hat{\sigma}_h$ | 2 | $\begin{pmatrix} -1 & 0 & 0 \\ 0 & 1 & 0 \\ 0 & 0 & 1 \end{pmatrix}$ | $\begin{pmatrix} 1 \\ 0 \\ 0 \end{pmatrix}, \begin{pmatrix} 0 \\ 1 \\ 0 \end{pmatrix}, \begin{pmatrix} 0 \\ 0 \\ 1 \end{pmatrix}$ | $\pi, 0, 0$ |
| Rotation, $\hat{r}_{n,m}$ | $n$ | $\begin{pmatrix} \cos(\theta) & -\sin(\theta) & 0 \\ \sin(\theta) & \cos(\theta) & 0 \\ 0 & 0 & 1 \end{pmatrix}$ | $\begin{pmatrix} 1 \\ +i \\ 0 \end{pmatrix}, \begin{pmatrix} 1 \\ -i \\ 0 \end{pmatrix}, \begin{pmatrix} 0 \\ 0 \\ 1 \end{pmatrix}$ | $+\theta, -\theta, 0$ |
| Elliptical rotation, $\hat{e}_{n,m}$ | $n$ | $\begin{pmatrix} \cos(\theta) & -\sin(\theta)/\epsilon & 0 \\ \epsilon\sin(\theta) & \cos(\theta) & 0 \\ 0 & 0 & 1 \end{pmatrix}$ | $\begin{pmatrix} 1 \\ +i\epsilon \\ 0 \end{pmatrix}, \begin{pmatrix} 1 \\ -i\epsilon \\ 0 \end{pmatrix}, \begin{pmatrix} 0 \\ 0 \\ 1 \end{pmatrix}$ | $+\theta, -\theta, 0$ |
| Elliptical improper rotation, $\hat{s}_{n,m}$ | $\mathrm{LCM}(2,n)$ | $\begin{pmatrix} \cos(\theta) & -\sin(\theta)/\epsilon & 0 \\ \epsilon\sin(\theta) & \cos(\theta) & 0 \\ 0 & 0 & -1 \end{pmatrix}$ | $\begin{pmatrix} 1 \\ +i\epsilon \\ 0 \end{pmatrix}, \begin{pmatrix} 1 \\ -i\epsilon \\ 0 \end{pmatrix}, \begin{pmatrix} 0 \\ 0 \\ 1 \end{pmatrix}$ | $+\theta, -\theta, \pi$ |

**6) <u>Selection rules for chiral dichroism in HHG</u>**

This section presents an application of our multi-scale DS theory for analyzing enantio-sensitive HHG (*52*, *53*). In a recent work (*12*), it was shown that HHG driven by "synthetic chiral light" – i.e. light with electric field vector that does not exhibit any microscopic DS involving reflection, inversion or improper rotations – display enantio-sensitive HHG power spectrum in the near field. When the synthetic chiral light is also "globally chiral", i.e. it has the same handedness in the entire interaction region, the far-field HHG is also enantio-sensitive. The situation is less clear when the driving field is synthetically chiral, but not globally chiral. Later work (*39*) demonstrated that some such fields do exhibit far-field enantio-sensitive HHG spectra. We show below that multi-scale DS theory can be used for analyzing these cases, providing chiral dichroism (CD) selection rules and physical insight.

We first analyzed the field presented in Ref. (*39*) which is given by (see eq. 21-27 in Ref. (*39*)):

$$\vec{E}(t,X,Y) = E_\omega\left[E_x(X)\hat{x} - iE_y(Y)\hat{y}\right]e^{i(k_y Y-\omega t)} + E_{2\omega}E_z(X)\hat{z}e^{2i(k_y Y-\omega t+\phi)} + c.c. \quad (21)$$

where

$$\begin{aligned} E_x(X) &= \cos(\alpha)\cos(k_x X) \\ E_y(X) &= \sin(\alpha)\sin(k_x X) \\ E_z(X) &= \cos(\alpha)\cos(2k_x X) \end{aligned} \quad (22)$$

where $\alpha$ is the half cross angle between the beams propagating in the x-y plane, $E_{m\omega}$ is the amplitude of the $m\omega$ ($m = 1,2$) field and $k_x = \sin(\alpha)\,k$. The field is locally-chiral (i.e. has a nonzero degree of chirality (*54*)) but not globally-chiral (i.e. the sign of the field's chirality changes rapidly across the interaction region). Through numerical simulations, Ref. (*39*) found that some harmonic orders still exhibit large chiral dichroism in the far field that is anti-symmetric with respect to the propagation angle (Fig. 4 in Ref. (*39*)).

We show here that multi-scale DSs of the light-matter system lead to a selection rule of the chiral dichroism spectra that matches and explains this feature.

We have found that the field in Eq. (21) exhibits the following multi-scale symmetry: $\hat{\sigma}_{xz}\hat{\Sigma}$ , i.e. $\hat{\sigma}_{xz}\vec{E}(t,-X)=\vec{E}(t,X)$. The microscopic reflection $\hat{\sigma}_{xz}$ flips the handedness of the field; hence, the interaction of $\vec{E}(t,X)$ with a medium of randomly oriented left-handed chiral molecules is equivalent to the interaction of $\vec{E}(t,-X)$ with randomly oriented right-handed chiral molecules up to a microscopic reflection $\hat{\sigma}_{xz}$. Therefore, the induced polarization of the two ennatiomers exhibits the relation:

$$\hat{\sigma}_{xz}\vec{P}^{L}(t,-X)=\vec{P}^{R}(t,X) \tag{23}$$

Implementing eq. (7) of the main text on eq. (23) leads to:

$$\hat{\sigma}_{xz}\vec{F}^{L}(q_1\omega,-q_2k_x)=\vec{F}^{R}(q_1\omega,q_2k_x) \tag{24}$$

The chiral dichroism of the far field HHG is defined as

$$\begin{aligned} CD(q_1\omega,q_2k_x) &= 2\frac{I^{L}(q_1\omega,q_2k_x)-I^{R}(q_1\omega,q_2k_x)}{I^{L}(q_1\omega,q_2k_x)+I^{R}(q_1\omega,q_2k_x)} \\ &= 2\frac{\left|\vec{F}^{L}(q_1\omega,q_2k_x)\right|^2-\left|\vec{F}^{R}(q_1\omega,q_2k_x)\right|^2}{\left|\vec{F}^{L}(q_1\omega,q_2k_x)\right|^2+\left|\vec{F}^{R}(q_1\omega,q_2k_x)\right|^2} \end{aligned} \tag{25}$$

where $I^{L}$ ($I^{R}$) is the intensity of emission from the left (right) handed enantiomer. Using the relation in Eq. (24) we obtain.

$$\begin{aligned} CD(q_1\omega,-q_2k_x) &= 2\frac{\left|\vec{F}^{L}(q_1\omega,-q_2k_x)\right|^2-\left|\vec{F}^{R}(q_1\omega,-q_2k_x)\right|^2}{\left|\vec{F}^{L}(q_1\omega,-q_2k_x)\right|^2+\left|\vec{F}^{R}(q_1\omega,-q_2k_x)\right|^2} \\ &= 2\frac{\left|\hat{\sigma}_{xz}\vec{F}^{R}(q_1\omega,q_2k_x)\right|^2-\left|\hat{\sigma}_{xz}\vec{F}^{L}(q_1\omega,q_2k_x)\right|^2}{\left|\hat{\sigma}_{xz}\vec{F}^{R}(q_1\omega,q_2k_x)\right|^2+\left|\hat{\sigma}_{xz}\vec{F}^{L}(q_1\omega,q_2k_x)\right|^2} \\ &= -2\frac{\left|\vec{F}^{L}(q_1\omega,q_2k_x)\right|^2-\left|\vec{F}^{R}(q_1\omega,q_2k_x)\right|^2}{\left|\vec{F}^{L}(q_1\omega,q_2k_x)\right|^2+\left|\vec{F}^{R}(q_1\omega,q_2k_x)\right|^2}=-CD(q_1\omega,q_2k_x) \end{aligned} \tag{26}$$

Eq. (26) establishes the following selection rule for CD: for a given emitted harmonic with temporal frequency $q_1\omega$, the CD at opposite spatial frequencies $q_2k_x$ and $-q_2k_x$ have opposite sign. This feature is clearly seen in Fig. 4 of Ref. (*39*).

Next, we analyzed another field that is locally-chiral but not globally-chiral, which was described in the supplementary of Ref. (*12*) and analyzed in Ref. (*54*). The field is a superposition of two non-collinear counter-rotating bi-elliptical fields, which near the focus are given by (eq S34-S5 in SI of Ref. (*12*)):

$$\begin{aligned} \vec{E}_1(t,X,Y)=\frac{1}{2}E_{1,0}\exp(ik(sin(\alpha)\,X+cos(\alpha)\,Y)-i\omega t)\,(cos(\alpha)\,\hat{x}-sin(\alpha)\,\hat{y}+i\epsilon_1\hat{z}) \\ +c.c. \end{aligned} \tag{27}$$

$$\vec{E}_2(t,X,Y) = \frac{1}{2}E_{2,0}\exp(i2k(-sin(\alpha)\,X + cos(\alpha)\,Y) - i2\omega t)\,(cos(\alpha)\,\hat{x} + sin(\alpha)\,\hat{y} - i\epsilon_2\hat{z}) + c.c.$$

Where $E_{n,0}$ is the electric amplitude $\epsilon_n$ is the ellipticity of the two fields.

Through a rigorous analysis, we have found that the total field $\vec{E} = \vec{E}_1 + \vec{E}_2$ exhibits the following multi-scale DS $\hat{\imath}\hat{\tau}_{8,3}\hat{X}_{8,-1}$, that is it upholds the equation:

$$-\vec{E}\left(t + 3\frac{2\pi}{8\omega}, X - \frac{2\pi}{8k_x}, Y\right) = \vec{E}(t,X,Y) \tag{28}$$

The microscopic inversion operation flips the handedness of chiral field. Therefore, following similar argument as in the previous case, the induced polarization of the two enantiomers will have the relation:

$$\hat{\imath}\hat{\tau}_{8,3}\hat{X}_{8,-1}\vec{P}^L(t,X) = \vec{P}^R(t,X) \tag{29}$$

Which according to the multi-scale DS theory, specifically Eq. (7) in the main text, leads to:

$$-\vec{F}^L(q_1\omega, q_2k_x)e^{\frac{2\pi i(3q_1-q_2)}{8}} = \vec{F}^R(q_1\omega, q_2k_x) \tag{30}$$

Inserting the relation to CD:

$$\begin{aligned} CD(q_1\omega, q_2k_x) &= 2\frac{\left|\vec{F}^L(q_1\omega, q_2k_x)\right|^2 - \left|\vec{F}^R(q_1\omega, q_2k_x)\right|^2}{\left|\vec{F}^L(q_1\omega, q_2k_x)\right|^2 + \left|\vec{F}^R(q_1\omega, q_2k_x)\right|^2} \\ &= 2\frac{\left|\vec{F}^L(q_1\omega, q_2k_x)\right|^2 - \left|-\vec{F}^L(q_1\omega, q_2k_x)e^{\frac{2\pi i(3q_1-q_2)}{8}}\right|^2}{\left|\vec{F}^L(q_1\omega, q_2k_x)\right|^2 + \left|-\vec{F}^L(q_1\omega, q_2k_x)e^{\frac{2\pi i(3q_1-q_2)}{8}}\right|^2} \\ &= 2\frac{\left|\vec{F}^L(q_1\omega, q_2k_x)\right|^2 - \left|\vec{F}^L(q_1\omega, q_2k_x)\right|^2}{\left|\vec{F}^L(q_1\omega, q_2k_x)\right|^2 + \left|\vec{F}^L(q_1\omega, q_2k_x)\right|^2} = 0 \end{aligned} \tag{31}$$

leads to forbidden CD, as argued in Ref. (*12*) (note that this assumes that the interaction region is spatially broad and contains the spatial structure of the light).

Thus, our theory for multi-scale DSs can also be applied in the field of chiral light-matter interactions to explain ultrafast chiral dichroism in solid and molecular systems.

**REFERENCES AND NOTES**


1. D. M. Bishop, *Group Theory and Chemistry* (Dover Publications, 1993).

2. C. L. Tang, H. Rabin, Selection rules for circularly polarized waves in nonlinear optics. *Phys. Rev. B* **3**, 4025–4034 (1971).

3. R. W. Boyd, *Nonlinear Optics*, vol. 5 of *Electronics & Electrical* (Academic Press, ed. 3, 2003).

4. O. E. Alon, V. Averbukh, N. Moiseyev, Selection rules for the high harmonic generation spectra. *Phys. Rev. Lett.* **80**, 3743–3746 (1998).

5. K. M. Dorney, L. Rego, N. J. Brooks, J. San Román, C.-T. Liao, J. L. Ellis, D. Zusin, C. Gentry, Q. L. Nguyen, J. M. Shaw, A. Picón, L. Plaja, H. C. Kapteyn, M. M. Murnane, C. Hernández-García, Controlling the polarization and vortex charge of attosecond high-harmonic beams via simultaneous spin–orbit momentum conservation. *Nat. Photonics* **13**, 123–130 (2019).

6. C. Hernández-García, A. Turpin, J. San Román, A. Picón, R. Drevinskas, A. Cerkauskaite, P. G. Kazansky, C. G. Durfee, Í. J. Sola, Extreme ultraviolet vector beams driven by infrared lasers. *Optica* **4**, 520 (2017).

7. F. Kong, C. Zhang, H. Larocque, Z. Li, F. Bouchard, D. H. Ko, G. G. Brown, A. Korobenko, T. J. Hammond, R. W. Boyd, E. Karimi, P. B. Corkum, Vectorizing the spatial structure of high-harmonic radiation from gas. *Nat. Commun.* **10**, 2020 (2019).

8. E. Frumker, N. Kajumba, J. B. Bertrand, H. J. Wörner, C. T. Hebeisen, P. Hockett, M. Spanner, S. Patchkovskii, G. G. Paulus, D. M. Villeneuve, A. Naumov, P. B. Corkum, Probing polar molecules with high harmonic spectroscopy. *Phys. Rev. Lett.* **109**, 233904 (2012).

9. D. Baykusheva, M. S. Ahsan, N. Lin, H. J. Wörner, Bicircular high-harmonic spectroscopy reveals dynamical symmetries of atoms and molecules. *Phys. Rev. Lett.* **116**, 123001 (2016).

10. S. Gholam-Mirzaei, J. Beetar, M. Chini, High harmonic generation in ZnO with a high-power mid-IR OPA. *Appl. Phys. Lett.* **110**, 061101 (2017).

11. O. Neufeld, D. Ayuso, P. Decleva, M. Y. Ivanov, O. Smirnova, O. Cohen, Ultrasensitive chiral spectroscopy by dynamical symmetry breaking in high harmonic generation. *Phys. Rev. X* **9**, 031002 (2019).

12. D. Ayuso, O. Neufeld, A. F. Ordonez, P. Decleva, G. Lerner, O. Cohen, M. Ivanov, O. Smirnova, Synthetic chiral light for efficient control of chiral light–matter interaction. *Nat. Photonics* **13** 866–871 (2019).

13. O. Neufeld, D. Podolsky, O. Cohen, Floquet group theory and its application to selection rules in harmonic generation. *Nat. Commun.* **10**, 405 (2019).

14. O. Kfir, P. Grychtol, E. Turgut, R. Knut, D. Zusin, A. Fleischer, E. Bordo, T. Fan, D. Popmintchev, T. Popmintchev, H. Kapteyn, M. Murnane, O. Cohen, Helicity-selective phase-matching and quasi-phase matching of circularly polarized high-order harmonics: Towards chiral attosecond pulses. *J. Phys. B At. Mol. Opt. Phys.* **49**, 123501 (2016).

15. A. Bahabad, M. M. Murnane, H. C. Kapteyn, Quasi-phase-matching of momentum and energy in nonlinear optical processes. *Nat. Photonics* **4**, 571–575 (2010).

16. L. Z. Liu, K. O'Keeffe, S. M. Hooker, Optical rotation quasi-phase-matching for circularly polarized high harmonic generation. *Opt. Lett.* **37**, 2415–2417 (2012).

17. D. Azoury, O. Kneller, M. Krüger, B. D. Bruner, O. Cohen, Y. Mairesse, N. Dudovich, Interferometric attosecond lock-in measurement of extreme-ultraviolet circular dichroism. *Nat. Photonics* **13**, 198–204 (2019).

18. E. Pisanty, L. Rego, J. San Román, A. Picón, K. M. Dorney, H. C. Kapteyn, M. M. Murnane, L. Plaja, M. Lewenstein, C. Hernández-García, Conservation of torus-knot angular momentum in high-order harmonic generation. *Phys. Rev. Lett.* **122**, 203201 (2019).

19. E. Pisanty, G. J. Machado, V. Vicuña-Hernández, A. Picón, A. Celi, J. P. Torres, M. Lewenstein, Knotting fractional-order knots with the polarization state of light. *Nat. Photonics* **13**, 569–574 (2019).

20. S. Xu, C. Wu, Space-time crystal and space-time group. *Phys. Rev. Lett.* **120**, 096401 (2018).

21. T. Janssen, A. Janner, Aperiodic crystals and superspace concepts. *Acta Crystallogr. Sect. B Struct. Sci. Cryst. Eng. Mater.* **70**, 617–651 (2014) .

22. V. S. Liu, B. K. Vanleeuwen, J. M. Munro, H. Padmanabhan, I. Dabo, V. Gopalan, D. B. Litvin, Spatio-temporal symmetry—Crystallographic point groups with time translations and time inversion. *Acta Crystallogr. Sect. A Found. Adv.* **74**, 399–402 (2018).

23. D. Shechtman, I. Blech, D. Gratias, J. W. Cahn, Metallic phase with long-range orientational order and no translational symmetry. *Phys. Rev. Lett.* **53**, 1951–1953 (1984).

24. R. Lifshitz, A. Arie, A. Bahabad, Photonic quasicrystals for nonlinear optical frequency conversion. *Phys. Rev. Lett.* **95**, 133901 (2005).

25. Z. V. Vardeny, A. Nahata, A. Agrawal, Optics of photonic quasicrystals. *Nat. Photonics* **7**, 177–187 (2013).

26. D. B. Litvin, W. Opechowski, Spin groups. *Phys. Ther.* **76**, 538–554 (1974).

27. N. V. B. Aleksei Vasil'evich Shubnikov, *Colored Symmetry* (Pergamon Press, 1964).

28. R. L. E. Schwarzenberger, Colour symmetry. *Bull. London Math. Soc.* **16**, 216–229 (1984).

29. M. R. Dennis, Polarization singularities in paraxial vector fields: Morphology and statistics. *Opt. Commun.* **213**, 201–221 (2002).

30. M. V. Berry, Index formulae for singular lines of polarization. *J. Opt. A Pure Appl. Opt.* **6**, 675–678 (2004).

31. G. Gariepy, J. Leach, K. T. Kim, T. J. Hammond, E. Frumker, R. W. Boyd, P. B. Corkum, Creating high-harmonic beams with controlled orbital angular momentum. *Phys. Rev. Lett.* **113**, 153901 (2014).

32. M. Lewenstein, P. Balcou, M. Y. Ivanov, A. L'Huillier, P. B. Corkum, Theory of high-harmonic generation by low-frequency laser fields. *Phys. Rev. A* **49**, 2117–2132 (1994).

33. Y. Tang, K. Li, X. Zhang, J. Deng, G. Li, E. Brasselet, Harmonic spin–orbit angular momentum cascade in nonlinear optical crystals. *Nat. Photonics* **14**, 658–662 (2020).

34. N. Wang, H. Chen, K. H. Kuo, Two-dimensional quasicrystal with eightfold rotational symmetry. *Phys. Rev. Lett.* **59**, 1010–1013 (1987).

35. L. Hareli, L. Lobachinsky, G. Shoulga, Y. Eliezer, L. Michaeli, A. Bahabad, On-the-fly control of high-harmonic generation using a structured pump beam. *Phys. Rev. Lett.* **120**, 183902 (2018).

36. O. Kfir, P. Grychtol, E. Turgut, R. Knut, D. Zusin, D. Popmintchev, T. Popmintchev, H. Nembach, J. M. Shaw, A. Fleischer, H. Kapteyn, M. Murnane, O. Cohen, Generation of bright phase-matched circularly-polarized extreme ultraviolet high harmonics. *Nat. Photonics* **9**, 99–105 (2014).

37. O. Kfir, E. Bordo, G. Ilan Haham, O. Lahav, A. Fleischer, O. Cohen, In-line production of a bi-circular field for generation of helically polarized high-order harmonics. *Appl. Phys. Lett.* **108**, 211106 (2016).

38. O. Neufeld, O. Cohen, Background-free measurement of ring currents by symmetry-breaking high-harmonic spectroscopy. *Phys. Rev. Lett.* **123**, 103202 (2019).

39. D. Ayuso, A. F. Ordonez, P. Decleva, M. Ivanov, O. Smirnova, Enantio-sensitive unidirectional light bending. *Nat. Commun.* **12**, 1–9 (2021).

40. C. Hernández-García, J. A. Pérez-Hernández, T. Popmintchev, M. M. Murnane, H. C. Kapteyn, A. Jaron-Becker, A. Becker, L. Plaja, Zeptosecond high harmonic keV X-ray waveforms driven by midinfrared laser pulses. *Phys. Rev. Lett.* **111**, 033002 (2013).

41. T. T. Luu, M. Garg, S. Yu. Kruchinin, A. Moulet, M. T. Hassan, E. Goulielmakis, Extreme ultraviolet high-harmonic spectroscopy of solids. *Nature* **521**, 498–502 (2015).

42. J. Hamazaki, R. Morita, K. Chujo, Y. Kobayashi, S. Tanda, T. Omatsu, Optical-vortex laser ablation. *Opt. Express* **18**, 2144–2151 (2010).

43. K. Toyoda, K. Miyamoto, N. Aoki, R. Morita, T. Omatsu, Using optical vortex to control the chirality of twisted metal nanostructures. *Nano Lett.* **12**, 3645–3649 (2012).

44. S. Sederberg, F. Kong, F. Hufnagel, C. Zhang, E. Karimi, P. B. Corkum, Vectorized optoelectronic control and metrology in a semiconductor. *Nat. Photonics* **14**, 1–6 (2020).

45. T. S. Ho, S. I. Chu, J. V. Tietz, Semiclassical many-mode floquet theory. *Chem. Phys. Lett.* **96**, 464–471 (1983).

46. I. Martin, G. Refael, B. Halperin, Topological frequency conversion in strongly driven quantum systems. *Phys. Rev. X* **7**, 041008 (2017).

47. K. Drese, M. Holthaus, Floquet theory for short laser pulses. *Eur. Phys. J. D* **5**, 119–134 (1999).

48. C. Hernández-García, J. A. Pérez-Hernández, J. Ramos, E. C. Jarque, L. Roso, L. Plaja, High-order harmonic propagation in gases within the discrete dipole approximation. *Phys. Rev. A - At. Mol. Opt. Phys.* **82**, 033432 (2010).

49. L. Drescher, O. Kornilov, T. Witting, G. Reitsma, N. Monserud, A. Rouzée, J. Mikosch, M. J. J. Vrakking, B. Schütte, Extreme-ultraviolet refractive optics. *Nature* **564**, 91–94 (2018).

50. J. A. R. Samson, W. C. Stolte, Precision measurements of the total photoionization cross-sections of He, Ne, Ar, Kr, and Xe, in *Journal of Electron Spectroscopy and Related Phenomena* (Elsevier, 2002), vol. 123, pp. 265–276.

51. D. B. Litvin, *Magnetic Group Tables: 1-, 2- and 3-Dimensional Magnetic Subperiodic Groups and Magnetic Space Groups* (International Union of Crystallography, 2013).

52. R. Cireasa, A. E. Boguslavskiy, B. Pons, M. C. H. Wong, D. Descamps, S. Petit, H. Ruf, N. Thiré, A. Ferré, J. Suarez, J. Higuet, B. E. Schmidt, A. F. Alharbi, F. Légaré, V. Blanchet, B. Fabre, S. Patchkovskii, O. Smirnova, Y. Mairesse, V. R. Bhardwaj, Probing molecular chirality on a sub-femtosecond timescale. *Nat. Phys.* **11**, 654–658 (2015).

53. D. Baykusheva, H. J. Wörner, Chiral discrimination through bielliptical high-harmonic spectroscopy. *Phys. Rev. X* **8**, 031060 (2018).

54. O. Neufeld, M. Even Tzur, O. Cohen, Degree of chirality of electromagnetic fields and maximally chiral light. *Phys. Rev. A* **101**, 053831 (2020).